

Prediction of Deformation and Failure Anisotropy for Magnesium Sheets Under Mixed-Mode Loading



Dirk Steglich and Jacques Besson

Abstract Despite the attractive strength-to-weight ratio of magnesium alloys, the application of magnesium sheet structures is restricted. Its anisotropy, the tension–compression asymmetry (the so-called strength differential effect, SD effect) and its poor formability at room temperature challenge engineers. In the current contribution, the deformation and failure behaviour of the innovative magnesium alloy “E-form” AZ31 at room temperature is investigated by means of mechanical tests and respective numerical simulations. Tensile and modified Arcan tests are analysed by digital image correlation (DIC) techniques. Arcan tests impose shear stresses while bending tests are conducted to force simultaneously tensile and compressive stresses in a sample. Irreversible deformation is described by a two-yield surface model, which couples the micromechanical mechanisms of dislocation glide and deformation twinning. Anisotropic failure is modeled using a linear transformation of the strain rate, which allows for a fast and efficient assessment of forming operation.

Keywords Finite elements · Anisotropy · Plasticity · Asymmetry · Strength differential effect · Tensile tests

Introduction

Sheet forming and bending are widely used operations in manufacturing industries. These processes are more frequently applied to magnesium sheets in the last decades, since magnesium alloys bear attractive properties like lightweight, durability, low density attractive in the automotive, rail coach, and aerospace industry. The relative low ductility of the common magnesium alloys, however, demands for reliable prediction tools for the assessment of forming operations.

D. Steglich (✉)

Institute of Material Systems Modeling, Helmholtz-Zentrum Hereon, Max-Planck-Str. 1, 21502 Geesthacht, Germany
e-mail: dirk.steglich@hereon.de

J. Besson

Centre des Matériaux, UMR CNRS 7633, PSL Research University, Mines ParisTech, 91003 Evry Cedex, France

Efforts were made for investigating the dependency of fracture on stress states. The relationship between ductile fracture strain and stress triaxiality is known from the 70 s of the last century [1, 2], for steels, established using notched tensile samples. It is nowadays accepted that ductility is reduced with increasing stress triaxiality. Many ductile fracture models have been developed on this basis and applied in the past: micromechanical-based porous plasticity models [3, 4] as well as phenomenological-based continuum damage models [5, 6]. Despite their respective merits, these approaches are complex because they require finite element analysis, since stress states cannot be directly measured. With the emerging possibilities in digital image correlation techniques, however, strain states can be monitored on the surface, and the use of the strain state for predicting failure appears advantageous.

In this work, the plastic deformation and failure behaviour of a novel magnesium sheet material (AZ31 ‘E-form’) under quasi-static loading conditions at room temperature is studied. This task is pursued using a combined methodology of experimental tests and numerical modelling using finite element simulations. The experimental part includes tensile, compressive, Arcan-like mixed-mode tension tests, and three-point out-of-plane bending tests. Samples were fabricated and tested along the rolling direction (RD), along the transverse direction (TD) and in the case of tensile tests and bending samples additionally 45° to the RD (DD orientation).

The validation is conducted with the use of the finite element (FE) simulation code Zebulon (Z-Set) [7]. A two-yield surface model [8] is adopted to capture anisotropy and asymmetry of the material effectively. The anisotropy parameters are calibrated using mechanical tests. Failure is predicted by a criterion based on linear transforms of the strain caused by dislocation glide.

A magnesium alloy sheet ‘E-form’, Mg–3Al–Zn with an average thickness of 1.17 mm is used here. The main alloying elements are aluminum and zinc with an approximate weight proportion of 3% and 1%, respectively. The material exhibits a weak basal texture [9], which results in a less pronounced anisotropy compared to common magnesium alloys.

Plasticity and Failure Model

A phenomenological two-yield surface (2YS) model is adopted here, which can capture the tension–compression asymmetry and in-plane anisotropy. A symmetric (for glide mechanisms) and an asymmetric yield surface (for twinning mechanisms) are used. The effective stress and strain quantities are defined for each yield surface, namely, $\bar{\sigma}_g$ and $\bar{\varepsilon}_g$ for the glide yield surface, and $\bar{\sigma}_t$ and $\bar{\varepsilon}_t$ for the twinning yield surface. The strain increment is decomposed in an elastic, an inelastic due to glide, and an inelastic contribution due to twinning:

$$d\boldsymbol{\varepsilon} = d\boldsymbol{\varepsilon}^e + d\boldsymbol{\varepsilon}^p = d\boldsymbol{\varepsilon}^e + d\boldsymbol{\varepsilon}_g^p + d\boldsymbol{\varepsilon}_t^p. \quad (1)$$

The inelastic strains are computed from the respective yield surface assuming associated flow. For the description of the glide mechanisms, a Barlat91 [10] formulation is selected:

$$\phi_g = f_g - \tilde{\sigma}_g = \frac{1}{2} (|\beta_2 - \beta_3|^b + |\beta_3 - \beta_1|^b + |\beta_1 - \beta_2|^b)^{\frac{1}{b}} - \tilde{\sigma}_g = 0, \quad (2)$$

where $\tilde{\sigma}_g$ describes the isotropic hardening of the yield surface and b is the yield function exponent. β_1, β_2 , and β_3 are the principal values of a linearly transformed stress tensor β derived from the Cauchy stress B following

$$\beta = L : B, \quad (3)$$

with L including the coefficients of anisotropy.

The inelastic deformation due to twinning is governed by the asymmetric CPB06 [11] criterion:

$$\phi_t = f_t - \tilde{\sigma}_t = (|\delta_1| - k\delta_1)^a + (|\delta_2| - k\delta_2)^a + (|\delta_3| - k\delta_3)^a)^{\frac{1}{a}} - \tilde{\sigma}_t = 0, \quad (4)$$

a being a scalar parameter, δ_1, δ_2 , and δ_3 are the principal values of a linearly transformed stress deviator, δ ,

$$\delta = M : T : \sigma. \quad (5)$$

T is the fourth-order tensor that transforms the stress tensor to its deviator and M is the fourth-order tensor including anisotropy parameters.

The interaction between two deformation mechanisms is achieved through a coupling of the respective hardening laws:

$$\tilde{\sigma}_g(\bar{\varepsilon}_g, \bar{\varepsilon}_t) = R_g + H_g \bar{\varepsilon}_t + Q_{1g} [1 - \exp(-b_{1g} \bar{\varepsilon}_g)] + Q_{2g} [1 - \exp(-b_{2g} \bar{\varepsilon}_g)], \quad (6)$$

$$\tilde{\sigma}_t(\bar{\varepsilon}_t) = R_t + H_t \bar{\varepsilon}_g + Q_{1t} [\exp(b_{1t} \bar{\varepsilon}_t) - 1]. \quad (7)$$

In Eqs. 6 and 7, $R_{g,t}, H_{g,t}, Q_{ig,t}, b_{ig,t}$ are scalar coefficients to be determined from mechanical tests.

In order to predict the onset of cracking in the samples, a strain-based damage criterion is selected using a scalar damage indicator:

$$D^e = \int H(\tilde{\dot{\varepsilon}}_I) \tilde{\dot{\varepsilon}}_I + H(\tilde{\dot{\varepsilon}}_{II}) \tilde{\dot{\varepsilon}}_{II} + H(\tilde{\dot{\varepsilon}}_{III}) \tilde{\dot{\varepsilon}}_{III} dt, \quad (8)$$

where H denotes the Heaviside function. The three principal strain rate components $\tilde{\dot{\epsilon}}_I$, $\tilde{\dot{\epsilon}}_{II}$, and $\tilde{\dot{\epsilon}}_{III}$, are used to define a damage indicator D^ϵ . For the description of the failure anisotropy, the strain rate components need to be transformed by a linear operator [12]. In the present case, the operator does not alter the deviatoric character of the transformed strain rate tensor $\tilde{\dot{\epsilon}}$:

$$\begin{bmatrix} \tilde{\dot{\epsilon}}_{11} \\ \tilde{\dot{\epsilon}}_{22} \\ \tilde{\dot{\epsilon}}_{33} \\ \tilde{\dot{\epsilon}}_{12} \end{bmatrix} = \frac{1}{9} \begin{bmatrix} 4L_1 + L_2 + L_3 & -2L_1 - 2L_2 + L_3 & -2L_1 + L_2 - 2L_3 & 0 \\ -2L_1 - 2L_2 + L_3 & L_1 + 4L_2 + L_3 & L_1 - 2L_2 - 2L_3 & 0 \\ -2L_1 + L_2 - 2L_3 & L_1 - 2L_2 - 2L_3 & L_1 + L_2 + 4L_3 & 0 \\ 0 & 0 & 0 & 9L_4 \end{bmatrix} \begin{bmatrix} \dot{\epsilon}_{11} \\ \dot{\epsilon}_{22} \\ \dot{\epsilon}_{33} \\ \dot{\epsilon}_{12} \end{bmatrix} \quad (9)$$

with four scalar coefficients L_1 , L_2 , L_3 , and L_4 .

Results

Parameter Calibration

The model parameters of the plasticity model are calibrated using an iterative optimisation procedure. Modified Arcan tests in 0° , 15° , 30° , and 45° configuration [9] with sample orientations along the RD and TD are considered for this purpose. Each test is modelled by FE simulations and the global response is compared to the experimentally obtained twin. By this procedure, the parameters listed in Table 1 are identified. The parameters describing shear components along the sheet thickness remain undetermined and hence are set to unity. Figure 1 shows the deformation–force record for the different configurations of the modified Arcan tests and the respective simulation. Table 1 gives the calibrated parameters.

Table 1 Optimised model parameters for the 2YS model and the failure criterion

Elasticity	$E = 43,000 \text{ MPa}$, $\nu = 0.3$
Glide	$b = 5.65$, $l^{LL} = 1$, $l^{TT} = 0.99$, $l^{SS} = 1.09$, $l^{TL} = 1.10$, $R_g = 116.4 \text{ MPa}$, $H_g = 848 \text{ MPa}$; $Q_{1g} = 58.3 \text{ MPa}$, $Q_{2g} = 116.4 \text{ MPa}$, $b_{1g} = 79.0 \text{ MPa}$, $b_{2g} = 13.3$
Twinning	$k = 0.9$, $a = 7.43$, $m^{LL} = 1.0$, $m^{TT} = 1.0$, $m^{SS} = -2.65$, $m^{LT} = 1.0$, $M^{TL} = -1.0$, $M^{TS} = -1.65$, $M^{SL} = -1.87$, $R_t = 45.0 \text{ MPa}$, $Q_{1t} = 54.4 \text{ MPa}$, $b_{1t} = 180$, $H_t = 1852 \text{ MPa}$
Failure	$L_1 = 4.02$, $L_2 = 5.87$, $L_3 = 1.0$, $L_4 = 2.42$

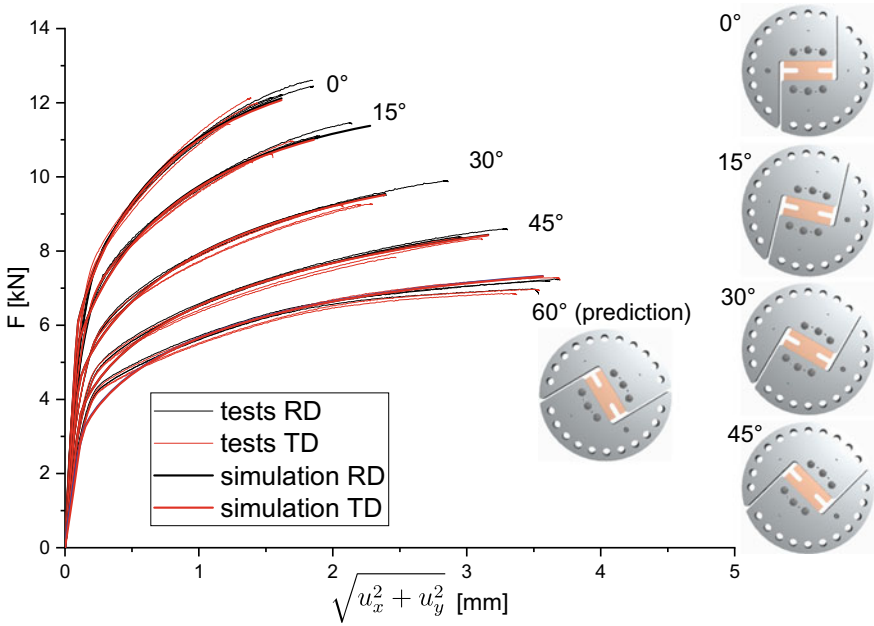


Fig. 1 Force–deformation behaviour of the Arcan samples

Prediction of Three-Point Bending

The model parameters of the 2YS model are validated by three-point bending tests (air bending). A rigid punch of 2 mm radius was symmetrically loading a metal strip of 10 mm width, bending it over cylindrical supports of 5 mm radius. The bending span was 18 mm. In the respective simulations, twofold symmetry was exploited for bending around the RD and TD axes and onefold symmetry for bending around the axis 45° from the RD (DD orientation).

Figure 2 shows the results in terms of global punch force as a function of displacement for the orientations RD, TD, and DD. The fit is excellent over the whole range of deformation and demonstrates the high predictive power of this model. Note that since there is no damage model coupled in the approach, the (early) drop of the load for failed samples is not envisaged to be captured.

Prediction of Crack Initiation

Three features related to failure were apparent during the mechanical tests:

1. Failure is of anisotropic nature, i.e. samples with main loading direction along the TD fail earlier than their counterparts loaded along the RD

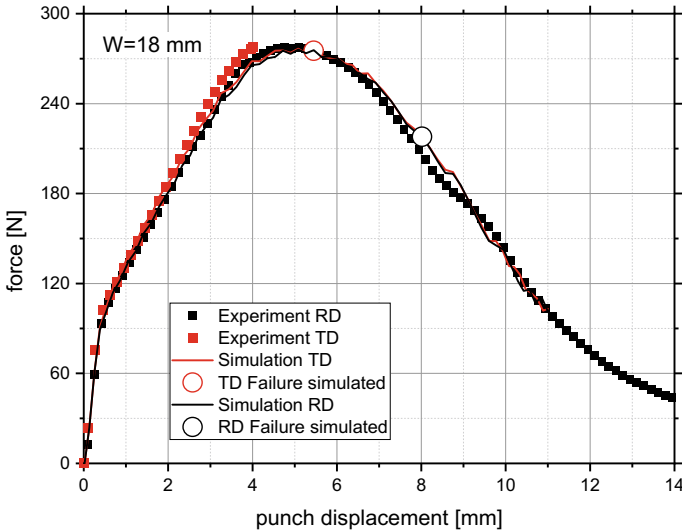


Fig. 2 Results of the three-point bending tests in terms of load vs. deflection; Crack initiation is indicated by symbols

2. With increasing orientation of the Arcan samples, failure is shifted to higher deformation
3. Cracking is initiated at the free surface of the notch; the position of crack initiation varies with the orientation angle.

Since the stress state is uniaxial at the edge of the sample, the selected initiation criterion is not accounting for the stress triaxiality. The parameters introduced in Eqn. [9] were calibrated using the macroscopic failure displacement norm $\sqrt{u_x^2 + u_y^2}$ (see Fig. 1). The results are presented in Fig. 3 together with the standard deviation of the repeated tests for each configuration.

All three features related to crack initiation are met by the simulations: The elevated ductility of samples loaded along the RD, the increase of global deformation with increasing loading angle, and the position of crack initiation of the Arcan samples, see Fig. 4.

It is worth mentioning that the failure criterion is aiming at predicting the onset of failure, i.e. the initiation location and stage of cracking. It is experimentally proven for the modified Arcan tests that crack initiation leads to an unstable crack extension, accompanied by a sudden drop of the external load. Hence, the prediction of the initiation suffices for establishing forming limits. A simulation of crack extension is not required for the assessment of forming operations.

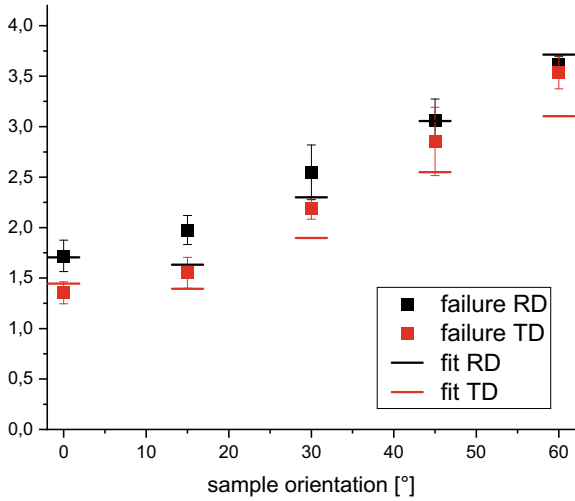


Fig. 3 Performance of the failure calibration in terms of displacement at failure (60° is prediction)

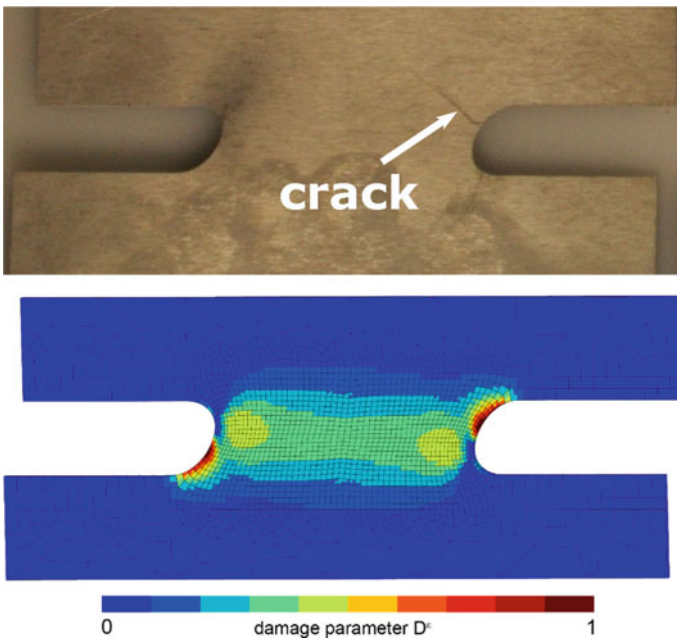


Fig. 4 Location of the crack initiation in case of the 45° TD sample; experiment (top) and damage indicator at the predicted failure load (bottom)

Conclusions and Outlook

The deformation and failure behaviour of a 3rd generation magnesium alloy AZ31 ‘e-form’ is explored by means of mechanical experiments and numerical simulations. In order to carry out a realistic simulation, a comprehensive experiment was established to characterise the material behaviour at room temperature. Using this database, material constitutive equations constituting anisotropy, elastoplastic behaviour with isotropic non-linear hardening was determined. An evolving anisotropy and a tension–compression asymmetry are quantified. While the stress anisotropy is less pronounced compared to other magnesium alloys, the strength differential effect is strong and has to be accounted for in the modelling of inelastic deformation.

A two-yield surface model (2YS) was constituted which allows good prediction of load vs displacement curves obtained from several mechanical tests in tensile and shear modes tests. The predictive power of the two-yield surface model is demonstrated. The model considers both deformation types, dislocation glide and mechanical twinning. This is particularly relevant in bending modes, since twinning is active in the zones undergoing compressive loadings.

A failure model based on the linear transformation of strain rates in the system of orthotropy was applied in order to assess the mechanical tests. It is able to predict the onset of failure, which was experimentally observed to start to form the edge of the Arcan samples. The model’s weakness of underestimating tensile failure along the RD is related to the strain localization in this particular test, see Fig. 5. While in the experiment little diffuse necking is observed (right part of Fig. 5), the simulation predicts localized necking with the maximum intensity of damage in the center of the sample (left part of Fig. 5).

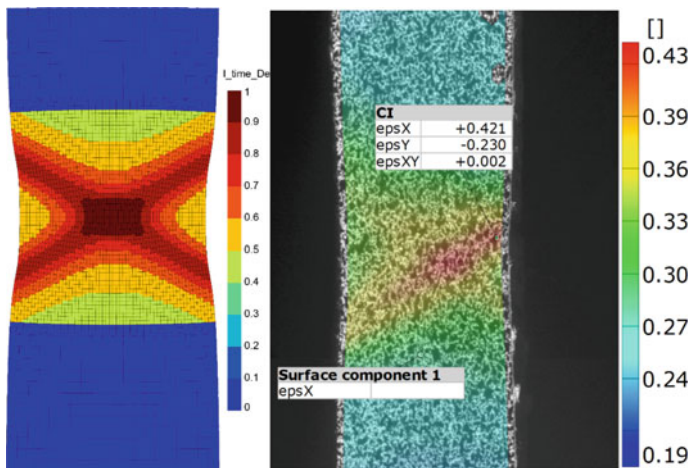


Fig. 5 Damage and strain localisation in a tensile experiment along the RD: damage indicator (left) at the predicted failure point, DIC image with axial logarithmic local strain prior to failure (right)

References

1. Hancock JW, Mackenzie AC (1976) On the mechanisms of ductile failure in high-strength steels subjected to multi-axial stress-states. *J Mech Phys Solids* 24:147–169
2. Mackenzie AC, Hancock JW, Brown DK (1977) On the influence of state of stress on ductile failure initiation in high strength steel. *Eng Fract Mech* 9:167–188
3. Gurson AL (1977) Continuum theory of ductile rupture by void nucleation and growth: part-1 yield criteria and flow rules for porous ductile media. *J Eng Mater Technol* 99:2–15
4. Tvergaard V, Needleman A (1984) Analysis of the cup-cone fracture in round tensile bar. *Acta Metall* 32:157–169
5. Lemaitre J (1985) A continuous damage mechanics model for ductile fracture. *J Eng Mater Technol-Trans Asme* 107:83–89
6. Rousselier G (1987) Ductile fracture models and their potential in local approach of fracture. *Nucl Eng Des* 105:97–111
7. Besson J, Foerch R (1997) Large scale object-oriented finite element code design. *Comput Methods Appl Mech Eng* 142:165–187
8. Steglich D, Tian X, Besson J (2016) Mechanism-based modelling of plastic deformation in magnesium alloys. *Eur J Mech A Solids* 55:289–303
9. Steglich D (2020) Mixed-mode deformation and failure of a magnesium sheet quantified using a modified arcan fixture. *Exp Mech* 60:109–118
10. Barlat F, Lege DJ, Brem JC (1991) A six-component yield function for anisotropic materials. *Int J Plast* 7:693–712
11. Cazacu O, Plunkett B, Barlat F (2006) Orthotropic yield criterion for hexagonal closed packed metals. *Int J Plast* 22:1171–1194
12. Jia Y, Bai Y (2016) Ductile fracture prediction for metal sheets using all-strain-based anisotropic eMMC model. *Int J Mech Sci* 115–116:516–531